



Levee breach-induced compound flood modeling

---

1 **Levee breach-induced compound flood modeling in Qianbujing Creek, Shanghai**  
2 **during Typhoon “Fitow”**

3

4 Yuhan Yang<sup>1</sup>, Jie Yin<sup>2,3,4\*</sup>, Weiguo Zhang<sup>1</sup>, Yan Zhang<sup>2</sup>, Yi Lu<sup>2</sup>, Aoyue Xiao<sup>2</sup>, Yunxiao Wang<sup>2</sup>,

5 Wenming Song<sup>2</sup>

6

7 <sup>1</sup> State Key Laboratory of Estuarine and Coastal Research, East China Normal University, China

8 <sup>2</sup> Key Laboratory of Geographic Information Science (Ministry of Education), East China Normal

9 University, China

10 <sup>3</sup> Department of Civil and Environmental Engineering, Princeton University, USA

11 <sup>4</sup> Institute of Eco-Chongming, East China Normal University, China

12 \* Correspondence to: J.Y. (email: jyin@geo.ecnu.edu.cn)

13

14 *Competing interests.* The authors declare that they have no conflict of interest.

15

16 **Abstract:** Levee breach-induced flooding occurs occasionally but always causes considerable

17 losses. A serious flood event occurred due to the collapse of a 15-m-long levee section in

18 Qianbujing Creek, Shanghai, China, during typhoon “Fitow” in Oct, 2013. Heavy rainfall

19 associated with the typhoon intensified the flood severity (extent and depth). This study

20 investigates the flood evolution to understand the dynamic nature of flooding and the compound

21 effect using a well-established 2D hydro-inundation model (Floodmap) to reconstruct this

22 typical event. Our simulation results provide a comprehensive view of the spatial patterns of



Levee breach-induced compound flood modeling

---

23 the flood evolution. The worst-hit areas are predicted to be low-lying settlement and farmland.  
24 Temporal evaluations suggest that the most critical time for flooding prevention is in the early  
25 hours after dike failure. In low-elevation areas, temporary drainage measures and flood  
26 defenses are equally important. The validation of the model demonstrates the reliability of the  
27 approach.

28

29 **Key words:** levee breach; compound flooding; inundation modeling; Shanghai

30

31

32

33

34

35

36

37

38

39

40

41

42

43

44



Levee breach-induced compound flood modeling

---

45 **1. Introduction**

46

47 Flooding is a common and devastating natural hazard, causing considerable personal injury,  
48 loss of life, and property damage worldwide (Jonkman et al., 2005; Jongman et al., 2012).  
49 Engineering measures such as dikes and barriers are typically constructed in low-lying deltas  
50 and floodplains to prevent flooding. However, weak or aging dikes without regular maintenance  
51 may fail during extreme flood events. Levee breaches may result in extensive flooding and  
52 damages throughout the hinterland (Ying et al., 2003). For example, Hurricane Katrina-induced  
53 flooding significantly damaged the dike system of New Orleans and overwhelmed the city,  
54 making it the costliest disaster in U.S. history (Kates et al., 2006). A more recent flood  
55 catastrophe with more than 50 deaths and hundreds of missing people resulted from of a dam  
56 breach due to a Himalayan glacier outburst flood in northern India.

57

58 In addition, riverine or storm-induced flooding is typically associated with heavy precipitation.  
59 The compound effect of pluvial, fluvial, or coastal flooding is much greater than the effect of  
60 individual flood events (Wahl et al., 2015). For instance, typhoon “Fitow” in 2013 brought  
61 torrential rain and caused high storm surge, resulting in record-breaking riverine water levels  
62 in the upstream region of the Huangpu River, Shanghai, China. As a result, the floodwall along  
63 the upstream Qianbujing Creek could not withstand the high water level, leading to a breach in  
64 a 15-m long section at 14:30 on 8 Oct 2013. Although the broken section was repaired after  
65 about 8 hours, the levee breach combined with heavy precipitation resulted in extensive flood  
66 inundation in the rural areas.



Levee breach-induced compound flood modeling

---

67

68 Over the last few decades, dike failure-induced flooding and the compound effect have received  
69 increasing attention from decision-makers, researchers and even general public. Recent studies  
70 have provided considerable progresses on dike reliability analysis and compound flood  
71 modeling (Curran et al., 2018; Naulin et al., 2018). A number of approaches for levee breach-  
72 induced flood modeling were developed. For example, Vorogushyn (2010) proposed an  
73 Inundation Hazard Assessment Model (IHAM), which coupled a 1D hydrodynamic model of  
74 river channel routing, a probabilistic dike breach model, and a 2D raster-based inundation  
75 model. Cannata et al. (2011) used a GIS-based approach to simplify a 2D dam break simulation.  
76 Yin et al. (2020) predicted dike failures and flood inundations in Shanghai, China, under various  
77 emission scenarios using an interdisciplinary process-based approach.

78

79 Similarly, numerous studies analyzed the compound effects of various flood hazards at different  
80 scales (Ganguli et al., 2020). Lian et al (2013) evaluated the combined effect of rainfall and the  
81 tidal level on flood risk in a complex river network in a coastal city in China. Moftehari et al  
82 (2017) proposed a bivariate flood hazard assessment approach to account for compound  
83 flooding from river flow and coastal water level. Bevacqua et al (2019) predicted the increasing  
84 probability of compound flooding from precipitation and storm surges in Europe under  
85 anthropogenic climate change. At a global scale, Couasnon (2020) and Eilander (2020)  
86 explored the compound flood potential resulting from storm surges and riverine floods.

87

88 The above studies contributed significantly to the modeling or evaluation of dike failure-



Levee breach-induced compound flood modeling

---

89 induced flooding or compound flood risk. However, few studies investigated the compound  
90 influences of pluvial and levee breach-induced flooding or focused on the dynamic process and  
91 mechanism of these cases, what can guide the development of appropriate emergency response  
92 plans. Moreover, real-life cases of historical flooding events have not been adequately  
93 investigated but can demonstrate the feasibility and robustness of the model. To address the  
94 research gaps, this case study seeks to examine the changing nature of levee breach-induced  
95 compound flooding. A simple 2D hydro-inundation model Floodmap is used to simulate the  
96 process of the compound flood event that occurred in Qianbujing Creek to improve our  
97 understanding of the evolution of flood inundation. The results of the approach are validated  
98 by field measurements, including the inundation depth and the flood extent over time. The  
99 findings can provide support for decision-makers to develop flood adaptation measures.

100

101 **2. Materials and methods**

102

103 **2.1 Study area**

104

105 The study area is located at the junction of the Huangpu River and Qianbujing Creek in the  
106 upstream Huangpu River Basin, Shanghai, China. The rural area covers about 1.5 km<sup>2</sup> with  
107 majority of agricultural land and minority of human settlements. It is characterized with a mild  
108 and low-lying topography (with an average altitude of about 3 m above Wusong Datum). Due  
109 to its location, the study area has faced high flood risk from the river system; however, the  
110 heights of the flood defense measures are relatively low (i.e., a 50-year return period flood



Levee breach-induced compound flood modeling

---

111 protection standard) compared to the high floodwall (1000-year period flood protection  
112 standard) along the mid- and downstream urban regions of the Huangpu River (Yin et al., 2020).  
113 Furthermore, because the region has a northern subtropical monsoon climate, pluvial flood  
114 events caused by extreme rainfall, typically associated with typhoons, are frequently recorded  
115 during the flood season (June to September) (Yin & Zhang, 2015). Therefore, the risk of  
116 compound flooding from both riverine and pluvial sources is significantly higher than that in  
117 other locations. Figure 1 shows the location of the study area and the levee breach during  
118 typhoon “Fitow”.

119

120 **2.2 Data sources and processing**

121

122 **2.2.1 Topographic data**

123

124 We used a 6-m resolution digital surface model (DSM) of the study area constructed from  
125 images of the China Resource 3 satellite (ZY-3) and other high-resolution satellites. Since  
126 buildings and trees represent barriers to water flow and reduce the area available for water  
127 storage in the hydrodynamic model, we removed the non-topographic features (e.g., trees and  
128 buildings) according to the Google historical dataset of remote sensing images to generate a  
129 bare-earth digital elevation model (DEM) based on the Wusong Datum of Shanghai. (Fewtrell  
130 et al., 2010; Neal et al., 2011; Yu & Lane, 2006b). We further resampled the cell size of the  
131 bare-earth DEM from 6 m to 2 m using ArcGIS software to improve the spatial resolution of  
132 the flood inundation model. The simulation domain of the study area consisted of 0.3 million



Levee breach-induced compound flood modeling

---

133 cells with an area of nearly 1.26 km<sup>2</sup>.

134

135 **2.2.2 Precipitation and water level**

136

137 Time series of the precipitation and water level records during Typhoon “Fitow” were used as  
138 boundary conditions to simulate the hydrodynamic process of the levee breach-induced  
139 flooding and the rainfall runoff. The data are typically derived from the stage measurements at  
140 gauge stations or radar-based rainfall data. However, due to the small scale of the study area,  
141 the gauging records are considered to be more reliable. Thus, we collected the historical records  
142 of the precipitation and water level data at the nearest gauging station from 0:00 on 8 Oct to  
143 12:00 on 9 Oct 2013 for about 12 hours before and after the levee failure.

144

145 The station-based precipitation records (at one-hour intervals) were obtained from the  
146 Information Center of the Shanghai Meteorological Administration. The water level data (at 5  
147 min intervals) at the closest gauging station along the Huangpu River (i.e. Songpu Bridge  
148 gauging station at the upstream of the Huangpu River, about 4 km away from Qianbujing Creek )  
149 were provided by the Shanghai Municipal Water Administration. The time series of the rainfall  
150 and water level data interpolated from the gauging stations is shown in Figure 2. Heavy rainfall  
151 occurred four hours before the levee breach, with the maximum hourly rainfall exceeding 20  
152 mm/h, resulting in the high water level of the river. Due to the high rainfall and rising storm  
153 tide, the water level increased rapidly to nearly 4.8 m and caused the collapse of a 15-m-long  
154 floodwall section at about 14:30 on 8 Oct.



Levee breach-induced compound flood modeling

---

155

156 **2.2.3 Validation data**

157

158 Aerial images or field surveys of flood extent were not available for the study event. There was  
159 also a lack of water depth data from electronic gauges and flood incidents reported by the public.  
160 Therefore, we validated the model through the field investigation of high water marks in the  
161 study area. We visited the study area three times in 2020 and investigated the residential areas  
162 (house by house), roadways, and farmland mostly affected by the flood event. Validation data  
163 were collected using questionnaires, and the coordinates of the locations were recorded by GPS.  
164 However, since this flood event occurred more than 7 years ago, there are inherent uncertainties  
165 in the investigation due to the changing environment and people's fading memory for the details  
166 of the event. Similarly, people tend to exaggerate their injuries and losses during hazards; thus,  
167 questionnaires can be highly biased. Finally, we pinpointed 32 incidents in total where locations  
168 are confidently identified. Among the 32 observed inundation data, 14 were buildings, 10 were  
169 roadways, and 8 were farmland locations (Figure 3).

170

171 **2.3 Levee breach modeling**

172

173 In general, levee breach mechanisms mainly include structural instability failures and structural  
174 strength failures. The former mode includes horizontal instability and rotational instability,  
175 whereas the latter refers to the destruction of structures (Wang, 2016). Due to the configuration  
176 of the floodwalls and the soil structure in Shanghai, structural instability failures always occur





Levee breach-induced compound flood modeling

---

177 during low water levels when critical inundation is less likely. In this case, structural strength  
178 failure was considered the major reason for the levee breach in the study area, namely, the levee  
179 collapse under an excessive hydraulic load on the wall due to an extremely high water level or  
180 the uneven settlement of the floodwalls.

181

182 We identified the location of the levee breach from the historical news reports and through field  
183 investigation. The 15-m long levee breach was located at the junction of Qianbujing creek and  
184 the main channel of the Huangpu River. The remaining floodwall height (4.9 to 5 m above  
185 Wusong Datum) data were obtained from the Shanghai Municipal Institute of Surveying and  
186 Mapping. The data were then overlaid onto the original bare-earth DEM using the raster  
187 calculator in ArcGIS 10.6 software.

188

189 **2.4 Compound flood modeling**

190

191 The compound flood modeling was performed using a 2D hydro-inundation model (FloodMap)  
192 (Yu & Coulthard, 2015; Yu & Lane, 2006a; 2006b), which couples hydrological processes (e.g.,  
193 infiltration, evapotranspiration, and drainage) module with 2D surface flood inundation  
194 modeling. The Floodmap model provides an effective approach for compound flood simulation,  
195 allowing for more than one hydrological boundary condition, including pluvial, fluvial, coastal  
196 and groundwater sources. In this study, the compound effect of pluvial and fluvial flooding was  
197 investigated. The fluvial flood modeling and pluvial flood modeling are described in Sections  
198 2.4.1 and 2.4.2, respectively.



Levee breach-induced compound flood modeling

---

199

200 **2.4.1 Fluvial flood modeling**

201

202 For simulating the levee breach-induced flooding, a simplified flood inundation module based  
203 on a raster environment was used to solve the inertial form of the 2D shallow water equations.  
204 The module considered the mass and momentum exchange between the river flow and  
205 floodplain inundation and has been used to simulate the dynamic nature of flood routing and to  
206 extract potential flood maps (Yang et al., 2020; Yin et al., 2015). The 2D inundation model is  
207 similar to the inertial algorithm of Bates et al. (2010). The difference is the time-step calculation  
208 approach. The optimal time step is calculated using the subsequent iteration instead of using  
209 the time step of the next iteration calculated by the current iteration. The main structure of the  
210 model is presented below.

211

212 The Saint-Venant momentum equation without the convective acceleration has the following  
213 form:

214 
$$\frac{\partial q}{\partial t} + \frac{gh\partial(h+z)}{\partial x} + \frac{gn^2q^2}{R^{4/3}h} = 0 \quad (1)$$

215 where  $g$  is the acceleration of gravity,  $q$  is the flow per unit width,  $R$  is the hydraulic radius,  
216  $h$  is the water depth,  $z$  is the bed elevation, and  $n$  is Manning's roughness coefficient. For  
217 wide and shallow flows,  $R$  can be approximated with  $h$ . The equation discretized with respect  
218 to time is:

219 
$$\frac{q_{t+\Delta t} - q_t}{\Delta t} + \frac{gh_t\partial(h+z)}{\partial x} + \frac{gn^2q_t^2}{h_t^{7/3}} = 0 \quad (2)$$

220 The  $q_t$  in the friction term can be replaced by  $q_{t+\Delta t}$  to obtain the explicit expression in the



Levee breach-induced compound flood modeling

---

221 next time step:

$$222 \quad q_{t+\Delta t} = \frac{q_t - gh_t \Delta t \left( \frac{\partial(h_t+z)}{\partial x} \right)}{(1 + gh_t \Delta t n^2 q_t / h_t^{10/3})} \quad (3)$$

223 The flows in the  $x$ - and  $y$ -directions are decoupled and have the same form. The discharge is  
224 evaluated at the cell edges, and the depth is determined at the cell center. For model constancy  
225 and minimizing numerical diffusion, we use the forward Courant-Friedrichs-Lewy condition  
226 (FCFL), which was used by Yu & Lane (2011) for the diffusion-based version of FloodMap, to  
227 calculate the time step in the inertial model:

$$228 \quad \Delta t \leq \min \left( \frac{w d_i d_j n}{d_i^{1.67} (S_i)^{1/2} + d_j^{1.67} (S_j)^{1/2}} \right) \quad (4)$$

229 where  $w$  represents the cell size,  $i$  and  $j$  are the indices for the flow direction in the  $x$ - and  
230  $y$ -directions,  $d_i$  and  $d_j$  are the effective water depths;  $S_i$  and  $S_j$  are the water surface  
231 slopes. The effective water depth is defined as the difference between the high water surface  
232 elevation and the high bed elevation of two cells that exchange water. The minimum time step  
233 that satisfies the FCFL condition for all wet cells is used as the global time step for this iteration.  
234 This approach does not require the back-calculation of the Courant number because the time  
235 step is calculated based on the CFL condition that satisfies every wet grid cell for the current  
236 iteration. The universal time step calculated with the FCFL may need to be scaled further by a  
237 coefficient with a value between 0 and 1 because the FCFL condition is not strictly the right  
238 stability criteria for an inertial system. A scaling factor in the range of 0.5–0.8 was found to  
239 yield a stable solution in previous studies; here, a scaling factor of 0.7 was used for all  
240 simulations. The calibration and validation of the model for the study area were conducted by  
241 Yin et al. (2016).

242



Levee breach-induced compound flood modeling

---

243 **2.4.2 Pluvial flood modeling**

244

245 In terms of the pluvial flooding module, we ran the surface water flood routing using the same  
246 structure as the fluvial flooding module. The infiltration over saturation was calculated by the  
247 widely used Green-Ampt equation, and the evapotranspiration was represented using a simple  
248 seasonal sine curve of daily potential evapotranspiration (Calder et al., 1983). This module also  
249 considered the amount of runoff loss to the urban storm sewer systems by scaling the drainage  
250 capacity (mm/h) for each time step.

251

252 The infiltration over saturation was determined by the widely used Green–Ampt equation,  
253 which approximates the rate of infiltration as a function of the capillary potential, porosity,  
254 hydraulic conductivity, and time using the following form:

255 
$$f(t) = K_s \left( \frac{\varphi_f + h_o}{z_f} + 1 \right) \quad (5)$$

256 where  $K_s$  expresses the hydraulic conductivity of the saturated soil,  $\varphi_f$  is the capillary  
257 potential across the wetting front,  $h_o$  is the water ponding on the soil surface, and  $z_f$  is the  
258 cumulative depth of infiltration.

259

260 The evapotranspiration was determined using a simple seasonal sine curve of daily potential  
261 evapotranspiration (Calder et al., 1983) as follows:

262 
$$E_p = \overline{E_p} \left[ 1 + \sin \left( \frac{360i}{365} - 90 \right) \right] \quad (6)$$

263 where  $E_p$  is the mean daily potential evapotranspiration, and  $i$  is the day of the year. The  
264 mass lost to evapotranspiration is typically limited due to the short duration of urban pluvial



Levee breach-induced compound flood modeling

---

265 flooding.

266

267 We used the topography boundary conditions, flow boundary conditions, and precipitation  
268 boundary conditions as inputs to model a 36-h compound flood process, including the 12 h  
269 before and after the levee breach, and we assumed evapotranspiration of 3 mm/day. The soil  
270 hydraulic conductivity ( $K_s$ ) is an important but highly complex parameter used to calculate  
271 infiltration. Empirically-based correlation methods or in situ hydraulic laboratory  
272 measurements can be used to determine the value of  $K_s$ . Given the practical constraints, this  
273 study refers to previous flood simulations in Shanghai (Yin et al., 2016; Yin et al., 2015; Yu &  
274 Coulthard, 2015; Yu et al., 2016) and used the value of 0.001 m/h for the hydraulic conductivity.  
275 A relatively high roughness value ( $n = 0.06$ ) was used in the simulation, according to the type  
276 of cultivated land and crops in the study area. Since the Qianbujing creek is located in a rural  
277 area, we did not consider the urban storm drainage capacity in this simulation.

278

279 **3. Results**

280 **3.1 Time series of flood inundation**

281

282 Figure 4 shows the changes in the predicted flood inundation every 4 h during the event, and  
283 Figure 5 depicts time series of average water depth and flood extent. These results show the  
284 spatial and temporal evolution of the levee breach-induced compound flooding during typhoon  
285 “Fitow”. Prior to the levee breach, it is apparent from Figures 4 and 5 that heavy rainfall in the  
286 study area led to localized shallow waterlogging, mainly in the low-lying farmland and forests.



Levee breach-induced compound flood modeling

---

287 The inundation area reached its first peak in the early hours on 8 Oct, but the water retention  
288 time was very short due to the shallow water depth (< 15 cm). At around 11:00 am on 8 Oct,  
289 another short-term rainstorm with rainfall over 20 mm/h occurred. Shortly after the  
290 precipitation peak, the water level of Qianbujing Creek showed an increasing trend. The  
291 compound effects of tide rising and heavy rain made the water level soon reached nearly 4.8 m  
292 (Figure 2). Due to the high water pressure, the bearing capacity of the floodwall was exceeded,  
293 resulting in a 15-m breached section (at 14:30 pm). Subsequently, overland flow through  
294 breached floodwalls and extensive flood inundation occurred quickly along the riverbank, first  
295 in the low-lying farmland near the river and then on roads and residential areas. About 10 homes  
296 were completely inundated during the water level rising period (until 16:00 p.m.) with the  
297 maximum inundation depth higher than 2 m. After 16:00 p.m., as the rainfall stopped and the  
298 water level dropped, the inundation area gradually stopped spreading.

299

300 A cross comparison of the derived flood hazard maps over time further indicated that although  
301 the rainstorm caused extensive surface water flooding in in majority of the study area, the  
302 inundation depth was generally shallow (< 15 cm). This effect can be attributed to the  
303 evapotranspiration and infiltration in a few hours. However, unlike the short-term waterlogging  
304 caused by the rainstorm, the compound effects of the rainfall and levee breach-induced flood  
305 inundation continued over 12 h, with an average water depth of nearly 60 cm.

306

307 **3.2 Maximum flood inundation**

308



#### Levee breach-induced compound flood modeling

---

309 The maximum flood extent and inundation during the event is shown in Figure 6. We use 2 cm  
310 as the threshold for surface water flooding and treat water depths shallower than 2 cm as sheet  
311 flow, which did not accumulate in topographic lows (Yu et al., 2016). Figure 6 shows that over  
312 half (56%) of the study area inundated from the compound flooding, and most of the flooded  
313 areas were low-lying farmland with maximum flood depths of higher than 2 m. Aside from the  
314 waterfront areas, many low-lying farmland areas were affected by the rainstorm, with  
315 maximum water depths over 50 cm. In contrast, the water depth on the roads and the buildings  
316 was shallow; most of it was less than 0.5 m and disappeared quickly. In nearly half of the  
317 flooded locations, the water depths were between 2 cm and 15 cm (44.1%), and a smaller  
318 proportion of the area (21.12%) had water depths between 15 cm to 50 cm. About 33.26% of  
319 the inundated areas had water depths of 50 cm to 2 m. In combination with the time series of  
320 water level and rainfall (Figure 2), It can be inferred that the maximum flood inundation  
321 occurred at about the fourth hour after the levee breaching (at ~16:00 p.m.) in waterfront area,  
322 while it occurred at about 11:30 a.m. in other areas.

323

### 324 **3.3 Model validation**

325

326 The field measurements were used to validate the performance of the compound flooding model.  
327 Figure 6 shows the location of the measurement points. The points were divided into building,  
328 road, and farmland types. Since there are few residential areas in the study area, reliable  
329 inundation information could not be obtained in most flooding areas; therefore, most of the  
330 points represent buildings with extensive inundation. Since there were uncertainties and errors



Levee breach-induced compound flood modeling

---

331 in the survey results, including the respondents' memory bias, exaggeration of inundation, and  
332 false positives, we set the observed error to 5 cm for building points, 10 cm for road points, and  
333 15 cm for farmland points. The simulation error was set as 5 cm. Figure 7 shows the scatter plot  
334 of the simulated and observed water depth and the 95% confidence interval. A correlation was  
335 observed between the simulated water depth and observed water depth, and most points fell  
336 within the confidence band. The observed water depth was slightly higher than the simulated  
337 water depth, which may be attributed to the exaggeration of the water depth by the respondents.

338

339 **3.4 Sensitivity analysis**

340

341 The model sensitivity to Manning's roughness coefficient over time was analyzed. Several  
342 Manning's  $n$  values (0.01–0.1 at a 0.01 increment) were used for the roughness  
343 parameterization. The difference between the average water depth (Figure 8a) and the total  
344 inundation area (Figure 8b) predicted by the simulations with different  $n$  values was calculated  
345 on a cell-by-cell basis. The results indicate similar trends of the average water depth and  
346 inundation area for different roughness values and differences in the values. As the roughness  
347 increased, the average water depth decreased, and the difference was more pronounced at higher  
348 roughness values. For example, the maximum average depth decreased from 0.55 m to 0.61 m  
349 with an increase in the  $n$  value of 0.01 to 0.1. Interestingly, there were differences in the  
350 sensitivity to the roughness before and after the levee breach for the flood inundation extent.

351 The inundation area increased slightly as the roughness increased during the rainstorm and  
352 decreased with an increase in the  $n$  value during the levee breach when the river flooding was





Levee breach-induced compound flood modeling

---

353 the main force. These results demonstrate the sensitivity of the model to the roughness.

354

355 **4. Conclusion and discussion**

356

357 This study used a simple 2D hydro-inundation model (Floodmap) to investigate serious  
358 compound levee breach-induced flooding during the typhoon “Fitow”. The surface runoff  
359 caused by the rainstorm and river overflow were considered in the model. The following  
360 conclusions can be drawn from the simulation results. First, one key advantage of this modeling  
361 approach is the analysis of a single historic flood event. The flooding results showed the time  
362 series of the flooding extent and inundation depth, indicating that the farmland areas near the  
363 river had a very high flood risk. Pluvial flooding or fluvial flooding caused extensive damage  
364 to low-lying areas due to the lack of a drainage network, especially waterlogging of farmland.  
365 The maximum water depth was more than 2 m. Second, within 1-3 h after the dike failure, the  
366 floodwaters spread rapidly, and the inundation area and average water depth reached the peak  
367 value; thus, this is the key period for repairing the levee. Subsequently, the flood risk decreased  
368 as the water level dropped. However, the water does not drain rapidly only by infiltration or  
369 evaporation, and the waterlogging lasted for more than 12 h, resulting in loss of farmland with  
370 high vulnerability. Therefore, in addition to repairing the levee, it is necessary to remove the  
371 flood water in time using drainage measures, such as water pumps.

372

373 Model validation was a challenging aspect of this research. The topographic data resolution,  
374 land use, and land cover affect the simulation results. The validation data consisted of field



Levee breach-induced compound flood modeling

---

375 observations, and the uncertainty associated with incorrect recollections of the residents led to  
376 errors. It was assumed that the error ranged from 5 cm to 15 cm for different land uses. Most  
377 of the verification results matched the field observations and fell within the confidence band,  
378 demonstrating the model's reliability. Nevertheless, some of the simulated water depths were  
379 slightly smaller than the field observations, which was attributed to the exaggeration of the  
380 depth by the respondents.

381

382 Another important component of this study is the comparison of the predictions (flooding extent  
383 and average water depth) using different Manning's  $n$  values (from 0.01 to 0.1 at a 0.01 interval).  
384 The results demonstrated the model's strong sensitivity to roughness. Overall, the model  
385 exhibited good reliability for single and compound flood modeling. Future research on this  
386 topic should be improved for the following aspects to improve the model robustness. (1)  
387 Higher-resolution topography and hydrological boundary conditions should be used to  
388 represent typical flood conditions. (2) The drainage capacity could be modeled to provide a  
389 more reliable result. (3) Urban compound flood risks should be evaluated to help decision-  
390 makers develop effective emergency response plans and flood adaptation strategies.

391

392 **Data Availability Statement.** The raw and processed data from the co-authors' research  
393 findings cannot be shared at this time, as these data are also part of the ongoing research. The  
394 satellite remote sensing image came from the Google Earth open-source datasets  
395 (<https://earth.google.com/>);

396

397 **Author contributions.** YY and JY initiated and led this research. YY designed the flood event  
398 process, analyzed the performance of this model, and wrote the paper. JY provided history  
399 records of water level. WZ and JY gave the suggestion for this paper. YL dealt with the rainfall  
400 data. YZ, AX, YW and WS helped in collecting validation data.



Levee breach-induced compound flood modeling

---

401 **Acknowledgments**

402 This paper was supported by the National Natural Science Foundation of China (Grant no:  
403 51761135024, 41871164), the National Key Research and Development Program of China  
404 (Grant no: 2017YFE0107400) and the Shanghai Sailing Program (Grant No. 21YF1456900).

405

406 **Reference**

- 407 Bates, P. D., Horritt, M. S., & Fewtrell, T. J. J. o. H. (2010). A simple inertial formulation of  
408 the shallow water equations for efficient two-dimensional flood inundation modelling.  
409 *Journal of Hydrology*, 387(1-2), 33-45.
- 410 Bevacqua, E., Maraun, D., Vousdoukas, M. I., Voukouvalas, E., & Widmann, M. J. S. A. (2019).  
411 Higher probability of compound flooding from precipitation and storm surge in Europe  
412 under anthropogenic climate change. *Science Advances*, 5(9), eaaw5531.
- 413 Calder, I. R., Harding, R. J., & Rosier, P. T. W. J. J. o. H. (1983). An objective assessment of  
414 soil-moisture deficit models. *Journal of Hydrology*, 60(1-4), 329-355.
- 415 Cannata, M., & Marzocchi, R. (2011). Two-dimensional dam break flooding simulation: a GIS-  
416 embedded approach. *Natural Hazards*, 61(3), 1143-1159.
- 417 Couasnon, A., Eilander, D., Muis, S., Veldkamp, T. I. E., Ward, P. J. J. N. H., & Sciences, E.  
418 S. (2020). Measuring compound flood potential from river discharge and storm surge  
419 extremes at the global scale. *Natural Hazards and Earth System Sciences*, 20(2), 489-504.
- 420 Curran, A., De Bruijn, K. M., & Kok, M. (2018). Influence of water level duration on dike  
421 breach triggering, focusing on system behaviour hazard analyses in lowland rivers.  
422 *Georisk: Assessment and Management of Risk for Engineered Systems and Geohazards*,  
423 14(1), 26-40.
- 424 Eilander, D., Couasnon, A., Ikeuchi, H., Muis, S., Yamazaki, D., Winsemius, H. C., & Ward,  
425 P. J. J. E. R. L. (2020). The effect of surge on riverine flood hazard and impact in deltas  
426 globally. *Environmental Research Letters*, 15(10), 104007 (104012pp).
- 427 Fewtrell, T. J., Bates, P. D., Horritt, M., & Hunter, N. M. J. H. P. (2010). Evaluating the effect  
428 of scale in flood inundation modelling in urban environments. *Hydrological Processes*,  
429 22(26), 5107-5118.
- 430 Ganguli, P., Paprotny, D., Hasan, M., Güntner, A., & Merz, B. (2020). Projected Changes in  
431 Compound Flood Hazard From Riverine and Coastal Floods in Northwestern Europe.  
432 *Earth's Future*, 8(11). doi:10.1029/2020ef001752
- 433 Jongman, B., Ward, P. J., & Aerts, J. C. J. H. (2012). Global exposure to river and coastal  
434 flooding: Long term trends and changes. *Global Environmental Change*, 22(4), 823-835.  
435 doi:10.1016/j.gloenvcha.2012.07.004
- 436 Jonkman, S. N. (2005). Global perspectives of loss of human life caused by floods. *Natural  
437 Hazards*, 34(2), 151-175.
- 438 Lian, J. J., Xu, K., Hydrology, C. M. J., Sciences, E. S., & Discussions. (2013). Joint impact of  
439 rainfall and tidal level on flood risk in a coastal city with a complex river network: a case  
440 study of Fuzhou City, China. *Hydrology and Earth System Sciences*, 17(1), 679-689.
- 441 Moftakhari, H. R., Salvadori, G., AghaKouchak, A., Sanders, B. F., & Matthew, R. A. (2017).  
442 Compounding effects of sea level rise and fluvial flooding. *Proceedings of the National  
443 Academy of the Sciences of the United States of America*, 114, 9785-9790.



Levee breach-induced compound flood modeling

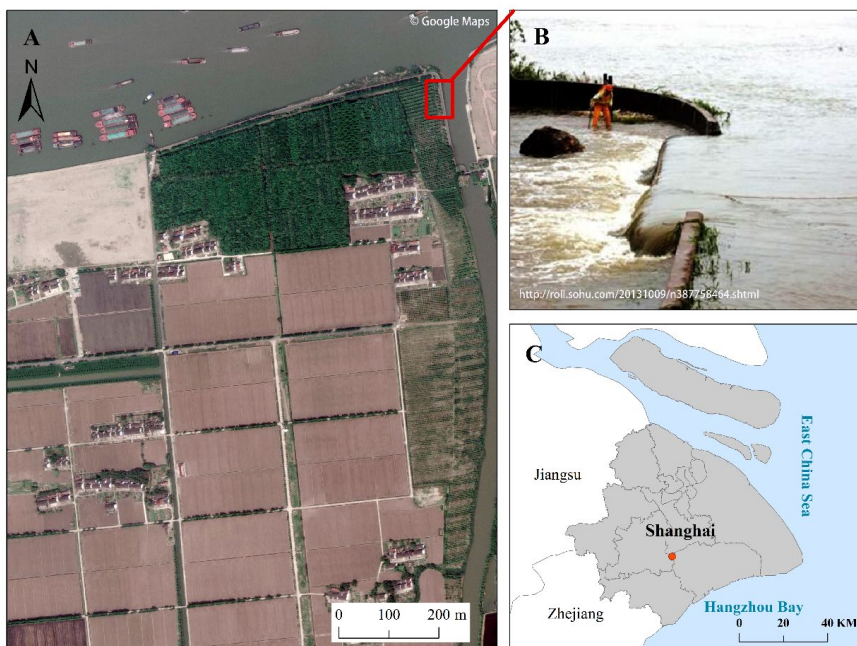
---

- 444 Naulin, M., Kortenhaus, A., & Oumeraci, H. (2018). Reliability-Based Flood Defense Analysis  
445 in an Integrated Risk Assessment. *Coastal Engineering Journal*, 57(1), 1540005-1540001-  
446 1540005-1540035.
- 447 Neal, J., Schumann, G., Fewtrell, T., Budimir, M., Bates, P., & Mason, D. J. J. o. F. R. M.  
448 (2011). Evaluating a new LISFLOOD-FP formulation with data from the summer 2007  
449 floods in Tewkesbury, UK. *Journal of Flood Risk Management*, 4(2).
- 450 Vorogushyn, S., Merz, B., Lindenschmidt, K. E., & Apel, H. (2010). A new methodology for  
451 flood hazard assessment considering dike breaches. *Water Resources Research*, 46(8).  
452 doi:10.1029/2009wr008475
- 453 Wahl, T., Jain, S., Bender, J., Meyers, S. D., & Luther, M. E. (2015). Increasing risk of  
454 compound flooding from storm surge and rainfall for major US cities. *Nature Climate  
455 Change*, 5(12), 1093-1097.
- 456 Yang, Y., Yin, J., Ye, M., She, D., & Yu, J. (2020). Multi-coverage optimal location model for  
457 emergency medical service (EMS) facilities under various disaster scenarios: a case study  
458 of urban fluvial floods in the Minhang district of Shanghai, China. *Natural Hazards and  
459 Earth System Sciences*, 20(1), 181-195.
- 460 Yin, J., Jonkman, S., Lin, N., Yu, D., & Wang, J. J. E. s. F. (2020). Flood Risks in Sinking  
461 Delta Cities: Time for a Reevaluation? *Earth's Future*, 8(8).
- 462 Yin, J., Yu, D., & Wilby, R. (2016). Modelling the impact of land subsidence on urban pluvial  
463 flooding: A case study of downtown Shanghai, China. *Science of the Total Environment*,  
464 544(July 2011), 744-753.
- 465 Yin, J., Yu, D., Yin, Z., Wang, J., Xu, S. J. L., & Planning, U. (2015). Modelling the  
466 anthropogenic impacts on fluvial flood risks in a coastal mega-city: A scenario-based case  
467 study in Shanghai, China. *Landscape and Urban Planning*, 136, 144-155.
- 468 Yin, J., & Zhang, Q. (2015). A comparison of statistical methods for benchmarking the  
469 threshold of daily precipitation extremes in the Shanghai metropolitan area during 1981–  
470 2010. *Theoretical and Applied Climatology*, 120(3-4), 601-607.
- 471 Ying, X., Wang, S. S. Y., & Khan, A. A. (2003). Numerical Simulation of Flood Inundation  
472 due to Dam and Levee Breach. Paper presented at the World Water & Environmental  
473 Resources Congress.
- 474 Yu, D., & Coulthard, T. J. J. J. o. H. (2015). Evaluating the importance of catchment  
475 hydrological parameters for urban surface water flood modelling using a simple hydro-  
476 inundation model. *Journal of Hydrology*, 524, 385-400.
- 477 Yu, D., & Lane, S. N. (2006a). Urban fluvial flood modelling using a two-dimensional  
478 diffusion-wave treatment, part 1: Mesh resolution effects. *Hydrological Processes*, 20(7),  
479 1541-1565.
- 480 Yu, D., & Lane, S. N. (2006b). Urban fluvial flood modelling using a two-dimensional  
481 diffusion-wave treatment, part 2: Development of a sub-grid-scale treatment. *Hydrological  
482 Processes*, 20(7), 1567-1583.
- 483 Yu, D., & Lane, S. N. (2011). Interactions between subgrid-scale resolution, feature  
484 representation and grid-scale resolution in flood inundation modelling. *Hydrological  
485 Processes*, 25(1), 36-53.
- 486 Yu, D., Yin, J., & Liu, M. (2016). Validating city-scale surface water flood modelling using  
487 crowd-sourced data. *Environmental Research Letters*, 11(12).



Levee breach-induced compound flood modeling

488



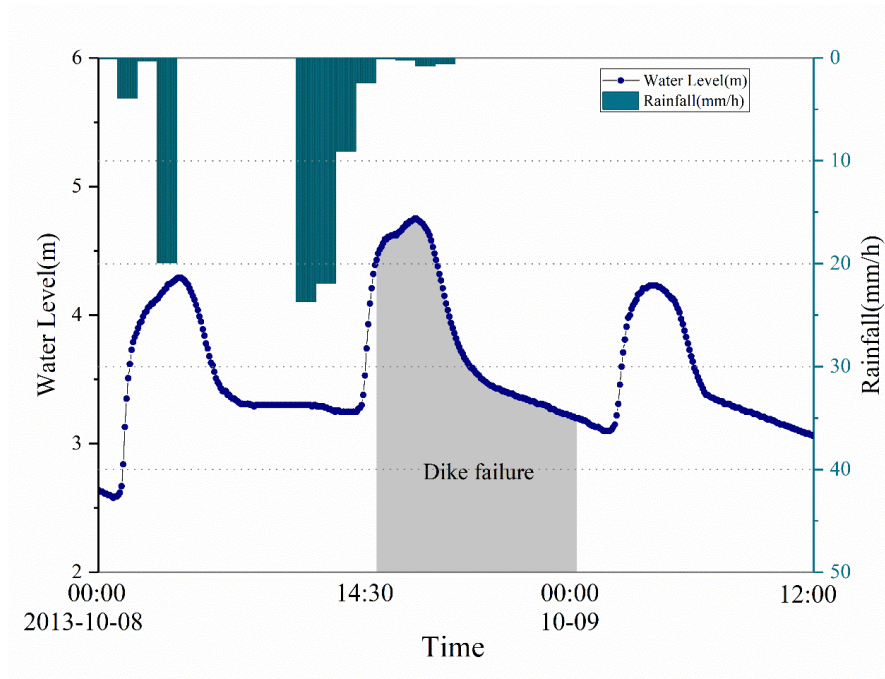
489

490

Fig. 1 Location of the study area and levee breach during typhoon “Fitow”



Levee breach-induced compound flood modeling



491

492 Fig.2 Time series of the water level and rainfall data at Qianbujing Creek during Typhoon

493 “Fitow”

494

495



Levee breach-induced compound flood modeling



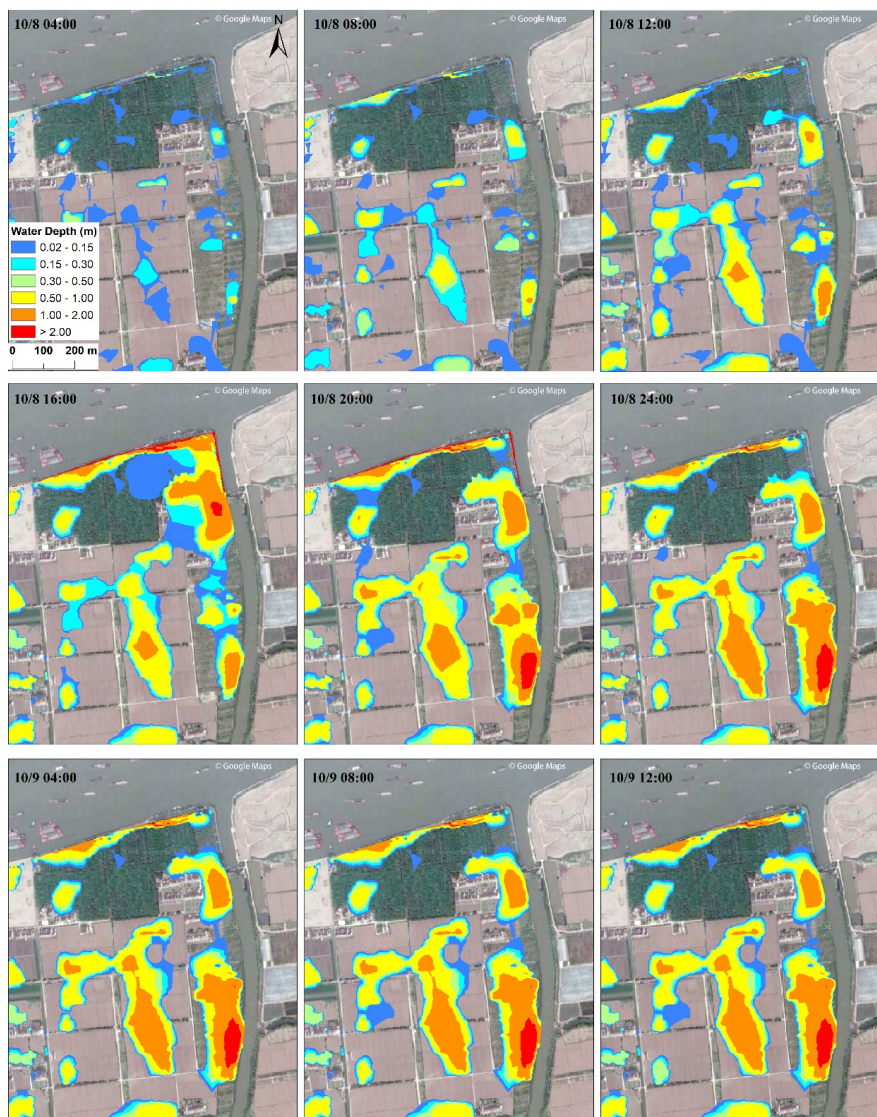
496

497

Fig. 3 Field investigation of flood inundation after the event



Levee breach-induced compound flood modeling



498

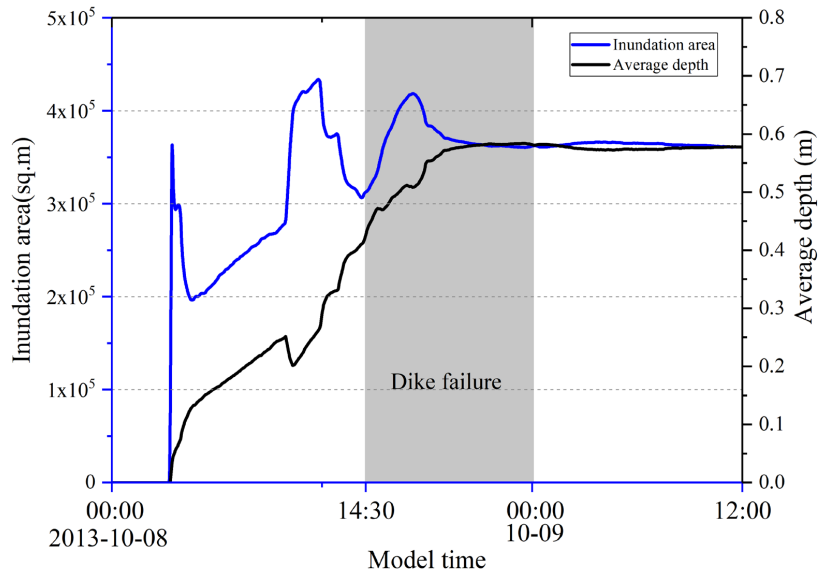
499

Fig. 4 Time series of flood inundation during the typhoon event





Levee breach-induced compound flood modeling



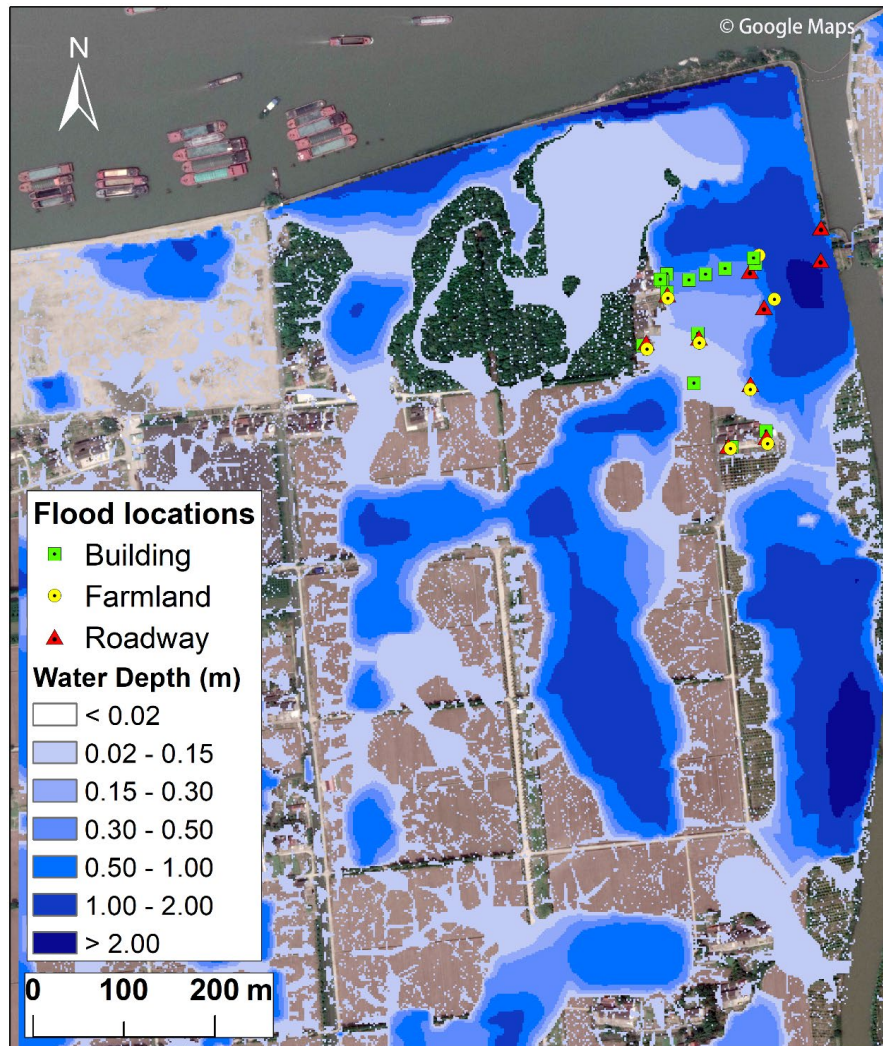
500

501

Fig. 5 Time series of the inundation area and water depth during the flood event



Levee breach-induced compound flood modeling



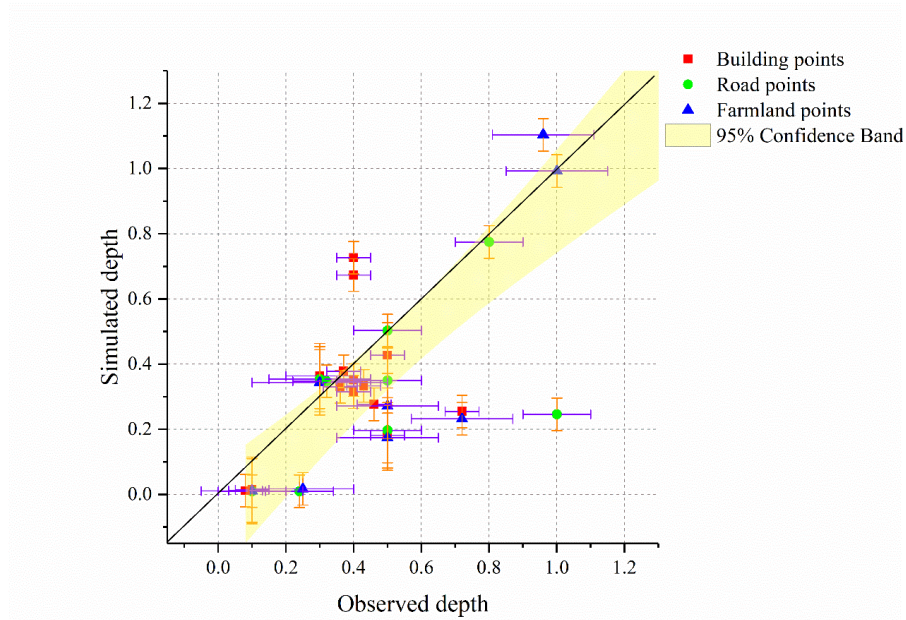
502

503

Fig. 6 Maximum flood extent and depth predicted by the model



Levee breach-induced compound flood modeling



504

505

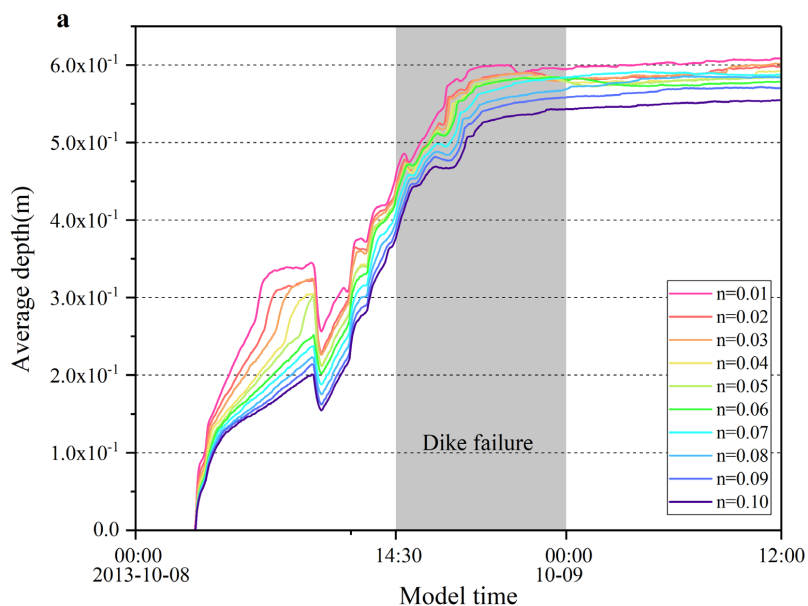
Fig. 7 A comparison of the simulated and observed depths

506

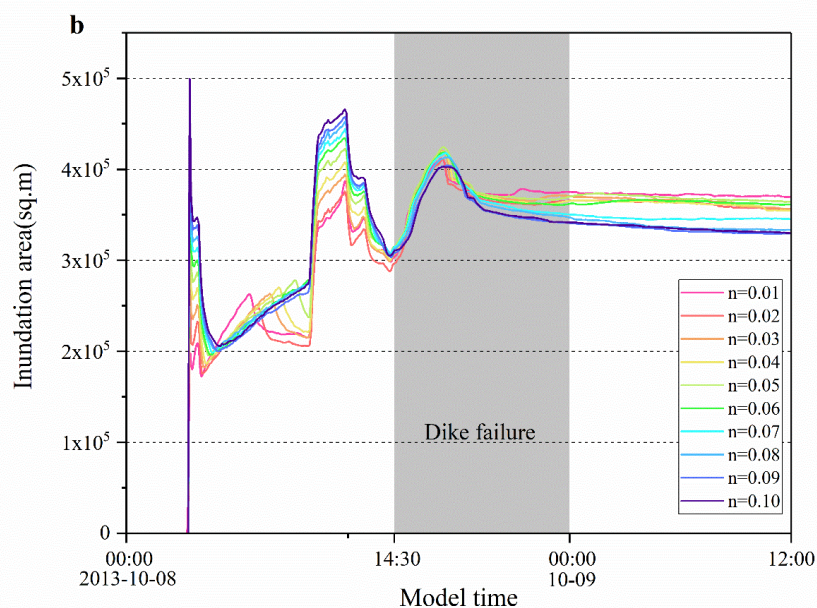
507



Levee breach-induced compound flood modeling



508



509

510

Fig. 8 Sensitivity analysis of the model to Manning's roughness coefficient